ZERO-OFFSET-BASED PRESTACK DIFFRACTION ENHANCEMENT USING A TRAVELTIME DECOMPOSITION APPROACH

A. Bauer, B. Schwarz, and D. Gajewski

email: *alex.bauer@uni-hamburg.de*

keywords: *diffractions, prestack, zero-offset, finite-offset, CRS*

ABSTRACT

Diffractions not only carry important information about small-scale subsurface structures, they also possess unique properties, which make them a powerful tool for seismic processing and imaging. Since a diffractor scatters an incoming wave to all directions, a diffraction event implies better illumination than a reflection, because the rays travel through larger parts of the subsurface. Furthermore, unlike the reflection case, in which the emergence location of the reflected wave depends on the source position, in the diffraction case Snell's law does not hold and, thus, up-going and down-going raypaths are decoupled. Based on this decoupling, we motivated a diffraction traveltime decomposition principle, which establishes a direct connection between zero-offset and finite-offset diffraction wavefield attributes. By making use of this approach, we are able to enhance diffractions and obtain high-quality diffraction wavefield attributes at arbitrary offsets in the prestack domain solely based on zero-offset processing without any further optimization. We show the accuracy of the method by fitting diffraction traveltimes and on simple waveform data. Application to complex synthetic data shows the ability of the proposed approach to enhance diffractions and provide high-quality wavefield attributes even in sparsely illuminated regions such as subsalt areas. The promising results reveal a high potential for improved prestack data enhancement and further applications such as efficient diffraction-based finite-offset tomography.

INTRODUCTION

Conventional seismic processing techniques are designed to image and enhance reflection events. However, reflected waves are not suitable for high-resolution structural imaging of features below the Rayleigh limit of half a seismic wavelength (e.g. Dell and Gajewski, 2011). Information about these small-scale structures such as edges, faults, pinch-outs and small-size scattering objects is encoded in the diffraction response of the subsurface (Khaidukov et al., 2004; Fomel et al., 2007). Therefore, the imaging of diffracted waves is a crucial challenge in seismic processing. Recently, different workflows with the goal to separate diffractions from reflections and to enhance diffractions in the post-stack domain have been presented (Fomel et al., 2007; Berkovitch et al., 2009; Dell and Gajewski, 2011). However, an important goal of diffraction imaging is the separation of diffractions and their enhancement in the full prestack data volume, which requires finite-offset (FO) processing. Finite-offset processing may provide improved resolution, especially in sparsely illuminated regions such as subsalt areas (Spinner et al., 2012). Due to the larger number of parameters the problem is of higher dimensionality, which makes processing less stable and computationally more expensive than in the zero-offset (ZO) setting.

In order to combine the stability of zero-offset CRS processing (Jäger et al., 2001) with the improved illumination of finite-offset processing, we recently introduced a straightforward decomposition principle for diffractions (Schwarz et al., 2014a; Bauer et al., 2014b). Based on the redundancy of zero-offset and

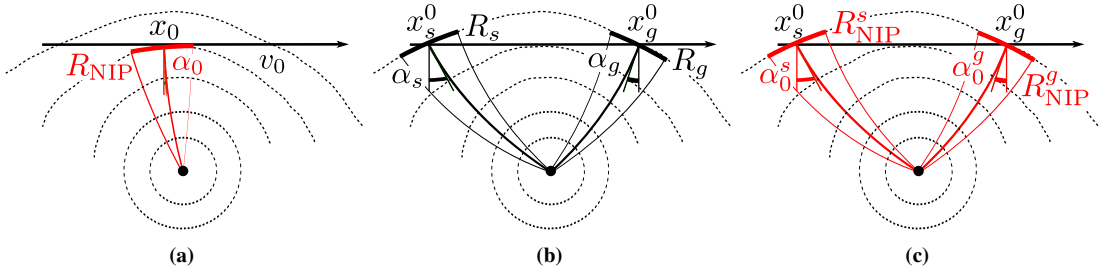

Figure 1: In the diffraction case, the zero-offset NIP-wave (a) approximates the actual physical wavefront. In the finite-offset setting (b), the common-shot (CS) and common-receiver (CR) experiments may be resembled by two independent zero-offset NIP-wave experiments (c) at source x_s^0 and receiver x_g^0.

finite-offset information for diffractions, this new approach allows the direct prediction of finite-offset diffraction attributes from zero-offset CRS processing results (Bauer, 2014; Bauer et al., 2015). In this fashion, the full prestack data volume is accurately characterized without carrying out computationally expensive generic finite-offset CRS processing (Zhang et al., 2001) or partial CRS stacking (Baykulov and Gajewski, 2009), where finite-offset traveltimes are extrapolated from zero-offset results.

THEORY

The common-reflection-surface (CRS) stack is a multi-parameter stacking technique, in which stacking is not only carried out along a traveltime moveout curve in offset direction, but along a traveltime moveout surface in both offset and midpoint direction (Jäger et al., 2001). CRS processing is purely data-driven and provides stacked sections with increased signal-to-noise ratio compared to the classical common-midpoint (CMP) stack, particularly in areas with complex geology and sparse illumination.

The CRS stack has been formulated for a central zero-offset (ZO) ray (Jäger et al., 2001) and for an arbitrary finite-offset (FO) central ray (Zhang et al., 2001). While the widely used zero-offset CRS stack is fast, stable and reasonably accurate for moderate lateral heterogeneity, finite-offset CRS shows its strengths in complex geological settings, where it provides improved resolution and illumination at the cost of being computationally more expensive and less stable (see, e.g., Spinner et al., 2012).

Zero-offset common-reflection-surface

In the reflection case, the 2D zero-offset CRS traveltime moveout depends on three parameters, the kinematic wavefield attributes α_0, R_{NIP} and R_{N} (Hubral, 1983). The latter ones, R_{NIP} and R_{N}, are the radii of two ficticious wavefronts, the NIP-wavefront and the normal wavefront. While the NIP-wave stems from a ficticious point source placed on the reflector's point of normal incidence (NIP, see Figure 1(a)), the normal wave is emitted by a ficticious exploding reflector segment around the NIP. The angle α_0 describes the direction from which the two ficticious waves emerge at the central midpoint. For the computation of the traveltime moveout along the CRS, different formulations exist (Müller, 1999; Jäger et al., 2001). In the special case of a diffraction the zero-offset traveltime moveout along the CRS only depends on two parameters, because the NIP-wave and the normal wave coincide. It is given by

$$t_{\mathrm{ZO}}(\Delta x_m, h) = t_0^{\mathrm{ZO}} + \frac{2\sin\alpha_0}{v_0}\Delta x_m + \frac{\cos^2\alpha_0}{v_0 R_{\mathrm{NIP}}}\left(\Delta x_m^2 + h^2\right) . \tag{1}$$

where $\Delta x_m = x_m - x_0$ is the displacement from the central midpoint x_0, h denotes the half-offset and v_0 is the constant near-surface velocity. As illustrated in Figure 1(a), the NIP-wave approximates the actual physical wavefront in the zero-offset section ($h = 0$),

$$t_{\mathrm{ZO}}(\Delta x_m) = t_0^{\mathrm{ZO}} + \frac{2\sin\alpha_0}{v_0}\Delta x_m + \frac{\cos^2\alpha_0}{v_0 R_{\mathrm{NIP}}}\Delta x_m^2 . \tag{2}$$

Based on the zero-offset CRS stack, Baykulov and Gajewski (2009) introduced the so-called partial CRS stack. In this method, finite-offset traces are simulated by application of zero-offset operators for local

finite-offset stacks, which corresponds to the extrapolation of traveltimes from zero-offset. Due to the smaller number of parameters this method is computationally more efficient than the generic finite-offset stack and in cases of moderate complexity and for small partial stacking apertures zero-offset operators perform reasonably well. However, the zero-offset approximation loses accuracy with increasing offsets and complexity. For moveout description at far offsets, finite-offset operators are more appropriate (see also Schwarz et al., 2014a; Bauer, 2014).

Finite-offset common-reflection-surface

The finite-offset CRS stack (Zhang et al., 2001) is a generalization of the zero-offset CRS stack to arbitrary source and receiver combinations, which allows the simulation of the full prestack data volume. Due to the higher dimensionality of the problem the finite-offset CRS stack cannot be parametrized by only three parameters. Instead, because of the asymmetry of up- and downgoing raypaths, the five finite-offset CRS parameters describe the attributes of the respective two-way wavefronts and a coupling coefficient, which can be considered as an expression of Snell's law. In the case of a diffraction, the coupling coefficient vanishes and thus the number of parameters reduces to four. Accordingly, the parabolic finite-offset response for diffractions in source ($x_s = x_m - h$) and receiver ($x_g = x_m + h$) coordinates is given by (Zhang et al., 2001)

$$\begin{aligned} t_{\text{FO}}(\Delta x_s, \Delta x_g) = t_0^{\text{FO}} &+ \frac{\sin\alpha_s}{v_s}\Delta x_s + \frac{1}{2}\frac{\cos^2\alpha_s}{v_s R_s}\Delta x_s^2 \\ &+ \frac{\sin\alpha_g}{v_g}\Delta x_g + \frac{1}{2}\frac{\cos^2\alpha_g}{v_g R_g}\Delta x_g^2 \,, \end{aligned} \tag{3}$$

where Δx_s and Δx_g denote the displacements from the central source and receiver pair (x_s^0, x_g^0) and v_s and v_g are the near surface velocities at x_s^0 and x_g^0. The coefficients of this second-order expression are parametrized by the emergence angles[1] α_s, α_g and the radii of curvature R_s, R_g of the wavefronts measured in the common-shot (CS) and common-receiver (CR) configurations, respectively.

Diffraction traveltime decomposition

Because of the decoupling of diffraction raypaths zero-offset and finite-offset information is redundant for diffractions (Schwarz et al., 2014a; Bauer et al., 2015): the CS and CR responses in a finite-offset measurement (see Figure 1(b)) are technically identical to two independent zero-offset measurements carried out at x_s^0 and x_g^0, as illustrated in Figure 1(c). Based on the assumption of reciprocity, which is valid for diffractions even in highly complex media, comparing equations (2) and (3) leads to the following system of equations:

$$\alpha_s = \alpha_0^s \,, \tag{4a}$$
$$\alpha_g = \alpha_0^g \,, \tag{4b}$$
$$R_s = R_{\text{NIP}}^s \,, \tag{4c}$$
$$R_g = R_{\text{NIP}}^g \,. \tag{4d}$$

The superscripts s and g indicate the zero-offset attributes measured at the central source and receiver position, respectively (compare Figure 1(c)). This system of equations establishes the relations between zero-offset and finite-offset diffraction attributes. Also the finite-offset reference traveltime can be expressed by the two zero-offset reference traveltimes,

$$t_0^{\text{FO}} = \frac{t_0^{\text{ZO},s} + t_0^{\text{ZO},g}}{2} \,. \tag{5}$$

Relations (4) and (5) indicate the redundancy of zero-offset and finite-offset information and thus allow the decomposition of any finite-offset operator into two independent zero-offset operators at a source x_s^0 and a

[1] Please note that we use a different sign convention for the emergence angles at source and receiver, which results in an alteration in signs compared to the original formula by Zhang et al. (2001)

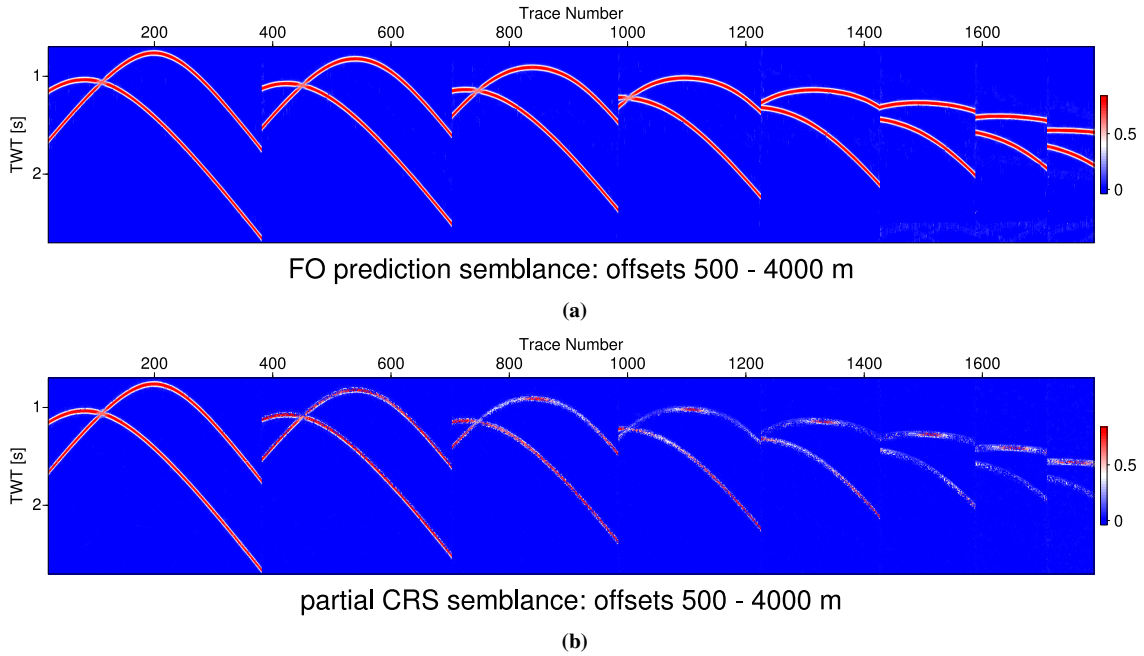

Figure 2: Finite-offset semblance sections of the simple waveform data for eight offsets from 500 (left) to 4000 m (right) generated by application of (a) the new diffraction traveltime decomposition approach and (b) the partial CRS method.

receiver x_g^0 (Schwarz et al., 2014a),

$$t_{\mathrm{FO}}(x_s^0, x_g^0, t_0^{\mathrm{FO}}, \alpha_s, \alpha_g, R_s, R_g) = \frac{t_{\mathrm{ZO}}(x_s^0, t_0^{\mathrm{ZO},s}, \alpha_0^s, R_{\mathrm{NIP}}^s)}{2} + \frac{t_{\mathrm{ZO}}(x_g^0, t_0^{\mathrm{ZO},g}, \alpha_0^g, R_{\mathrm{NIP}}^g)}{2} \,. \tag{6}$$

Since the traveltime decomposition principle is a fundamental property of diffractions, Equation (6) holds independently of the choice of zero-offset operators. If, e.g., hyperbolic operators are used during the zero-offset processing, the finite-offset diffraction operators composed according to (6) correspond to double-square-root operators (Yilmaz, 2001).

Given the zero-offset measurements are accurate, the introduced decomposition principle is exact for diffractions in arbitrary media and therefore, we also refer to it as *finite-offset prediction for diffractions*. Note that this decomposition principle is only valid for diffractions, because it is based on the assumption of decoupled up- and downgoing raypaths. In the reflection case, the previously introduced equations do not hold.

For the application to waveform data, we integrated the new diffraction traveltime decomposition approach into the zero-offset CRS workflow (Mann, 2002; Baykulov and Gajewski, 2009). As input, FO prediction requires the prestack data and results of the optimized zero-offset CRS stack, namely the optimized semblance and the attribute sections of the zero-offset wavefield attributes α_0 and R_{NIP}. In order to predict a finite-offset trace for the half-offset h_0 at the midpoint $x_m = x_0$, information from the locations $x_s^0 = x_0 - h_0$ and $x_g^0 = x_0 + h_0$ in the zero-offset section is required. At these locations, the two events which stem from the same diffractor have to be found and matched. In this implementation, different event combinations are tested in order to find the one which provides the best fit. For each sample t_0^{FO} of the finite-offset trace, the source and receiver traces are searched for the corresponding diffraction events using relation (5). In the current implementation, the event search is confined by the relation $\Delta t_0 \leq 2h_0/v_0$, which holds for the traveltime difference between the two events. For each event pair found, the four finite-offset wavefield attributes are extracted from the zero-offset attribute sections. They define the finite-offset diffraction operator for $(x_0, h_0, t_0^{\mathrm{FO}})$. The parameters are tested for accuracy by computing the coherence for the constructed operator. In contrast to the generic finite-offset CRS stack, only the already estimated zero-offset attribute pairs at source and receiver need to be combined.

As output, our method provides the finite-offset stacks, the respective semblance and the four finite-offset attribute sections for the predefined range of offsets. The method is able to handle an arbitrary number of conflicting events, if they are provided with the zero-offset results.

SIMPLE DATA EXAMPLE

In order to verify the proposed method on waveform data, we applied it to a simple dataset based on the same velocity model as the diffraction traveltime fit, but this time containing an additional diffractor at a depth of 1.5 km and lateral position of 3.5 km. The dataset contains a total of 401 CMPs and both the lateral extension of the seismic line and the maximum offset are 5 km. Figure 2 compares various finite-offset semblance sections ranging from 500 m to 4000 m offset provided by FO prediction and the zero-offset-based partial CRS method (Baykulov and Gajewski, 2009). The results clearly reveal that the zero-offset operators used by partial CRS (Figure 2(b)) lose accuracy with increasing offset, because they extrapolate traveltimes. However, the FO prediction results (Figure 2(a)) are of very high quality along the whole offset range, because the decomposed finite-offset operators are accurate for arbitrary offsets. The decomposition relations define the diffraction moveout globally, while the respective zero-offset-based operators are only accurate in local vicinities of each reference ray.

COMPLEX DATA EXAMPLE

2004 BP velocity benchmark

The 2004 BP velocity benchmark is a complex synthetic dataset introduced by Billette and Brandsberg-Dahl (2005). It is based on a velocity model which contains complex salt geometries to the left and in the center and a relatively shallow mud volcano structure surrounded by an increasing velocity gradient to the right of the profile line. The velocity model is displayed in Figure 3, where the dotted lines indicate the location of the excerpts presented in this section. The data was modeled including free-surface multiples and assuming a modern streamer acquisition including large offsets up to 15 km (Billette and Brandsberg-Dahl, 2005).

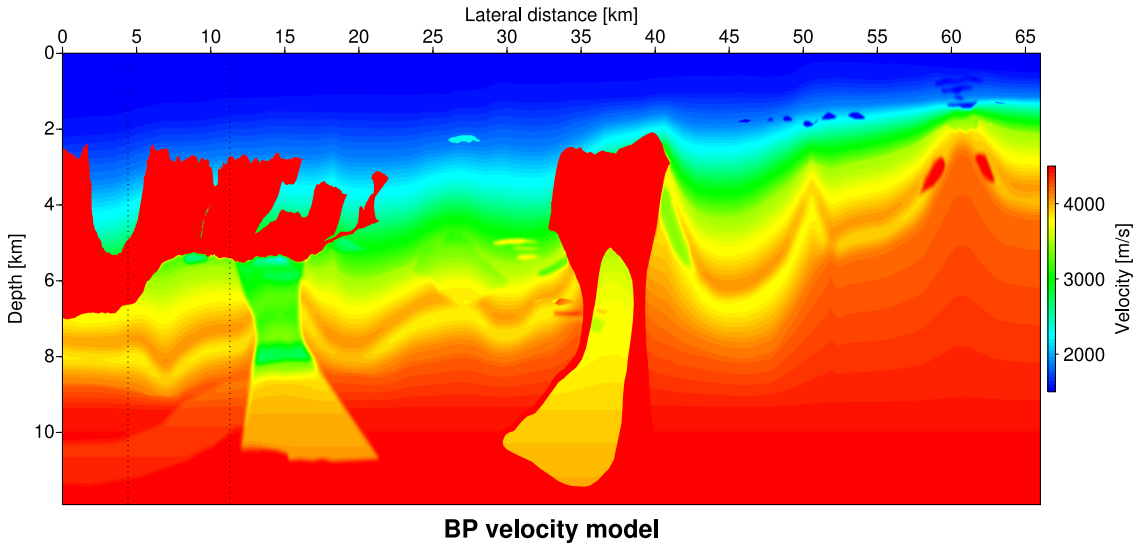

Figure 3: The 2004 BP velocity model (Billette and Brandsberg-Dahl, 2005). The dotted lines indicate the location of the excerpts shown in this work.

In order to test our method's ability to enhance diffractions in the prestack domain, we applied it to an excerpt of the BP velocity benchmark data. Figure 4 shows an excerpt of the unprocessed raw data according to the dotted lines in Figure 3 for four different finite-offsets (1, 3, 5 and 7 km, from left to right). The zero-offset CRS processing was carried out on the raw data using a global optimization scheme

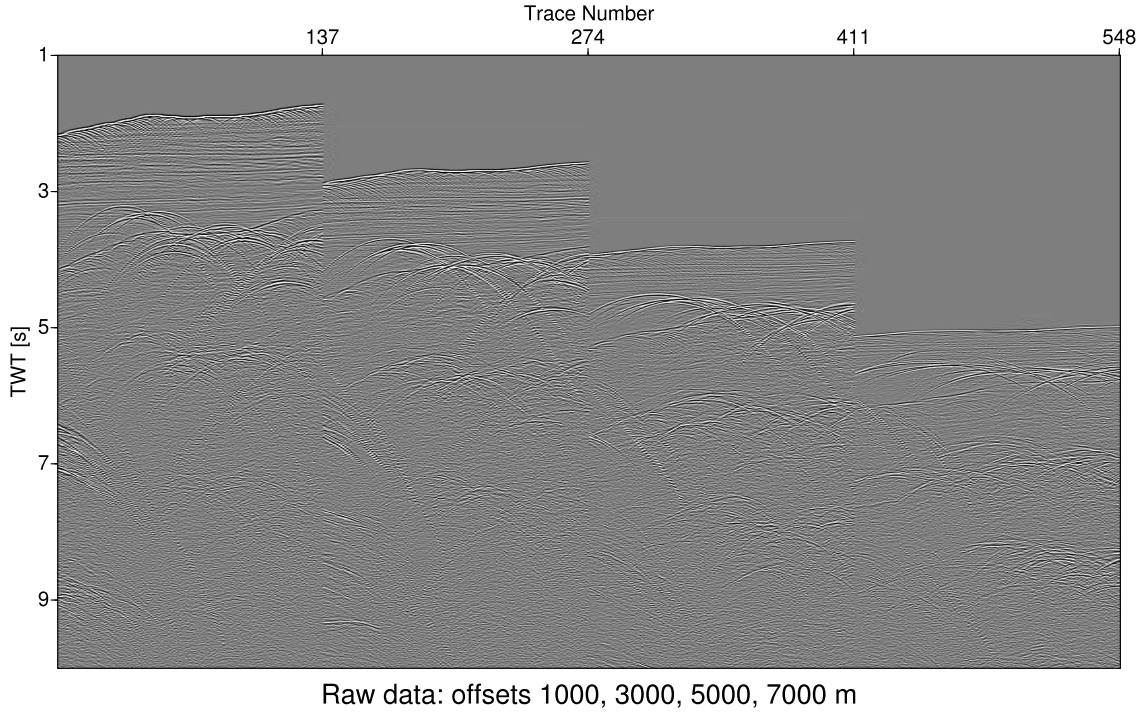

Figure 4: Excerpts of the raw 2004 BP velocity benchmark data for four offsets from 1000 (left) to 7000 m (right).

during the attribute search and allowing for a maximum of 21 conflicting dips at one time sample (Walda and Gajewski, 2015). Using the zero-offset CRS results as input, we applied the diffraction decomposition stack (Bauer et al., 2015) and partial CRS (Baykulov and Gajewski, 2009) to the data. Figure 5 shows excerpts of the resulting finite-offset stacked sections for the same four offsets (1, 3, 5 and 7 km) as obtained from FO prediction (above) and partial CRS (below). The results show that the diffraction decomposition approach is able to image diffractions accurately for the full considered offset range, whereas the quality of the partial CRS results in terms of diffractions strongly decreases with offset, in particular for weaker events at larger traveltimes. Comparing the FO prediction result (Figure 5(a)) to the prestack data (Figure 4) reveals a significantly increased signal-to-noise ratio of the diffracted waves recorded in the data.

Figure 6 shows the semblance sections corresponding to the stacks. The images clearly reveal the differences of the two considered methods and prove that the diffraction decomposition approach is able to image diffractions coherently at arbitrary offsets despite of being based entirely on zero-offset attributes. However, the zero-offset operators used by the partial CRS approach become more inaccurate with increasing offset, especially for diffractions. As a result, except for reflected waves stemming from nearly planar shallow structures such as the seafloor, almost no coherent energy is found by the method at larger offsets.

Since the decomposition relations (6) define the moveout of a diffraction globally, they allow us to obtain the exact finite-offset wavefield attributes at arbitrary locations in the prestack data cube. Prestack wavefield attributes may be utilized for further processing steps such as, e.g., stereotomography (Billette and Lambaré, 1998). Figure 7 exemplarily shows the finite-offset attributes α_s, the emergence angle at the source, and R_s, the radius of the diffraction wavefront emerging at the source, as obtained from FO prediction. Figure 7(a) reveals that especially the emergence angle is of high quality for all offsets, even for weak events recorded at large traveltimes. The wavefront curvature R_s (Figure 7(b)) appears more blurry than the angle, but still, most of the coherent diffraction events are clearly distinguishable. Since curvatures are wavefield attributes of second order, they are naturally less stable and more difficult to estimate during the zero-offset processing than angles, which are first order attributes. Please note that the finite-offset operators are gained by combining the previously estimated zero-offset operators at source and receiver. There is no further attribute search required. Accordingly, the diffraction decomposition directly benefits

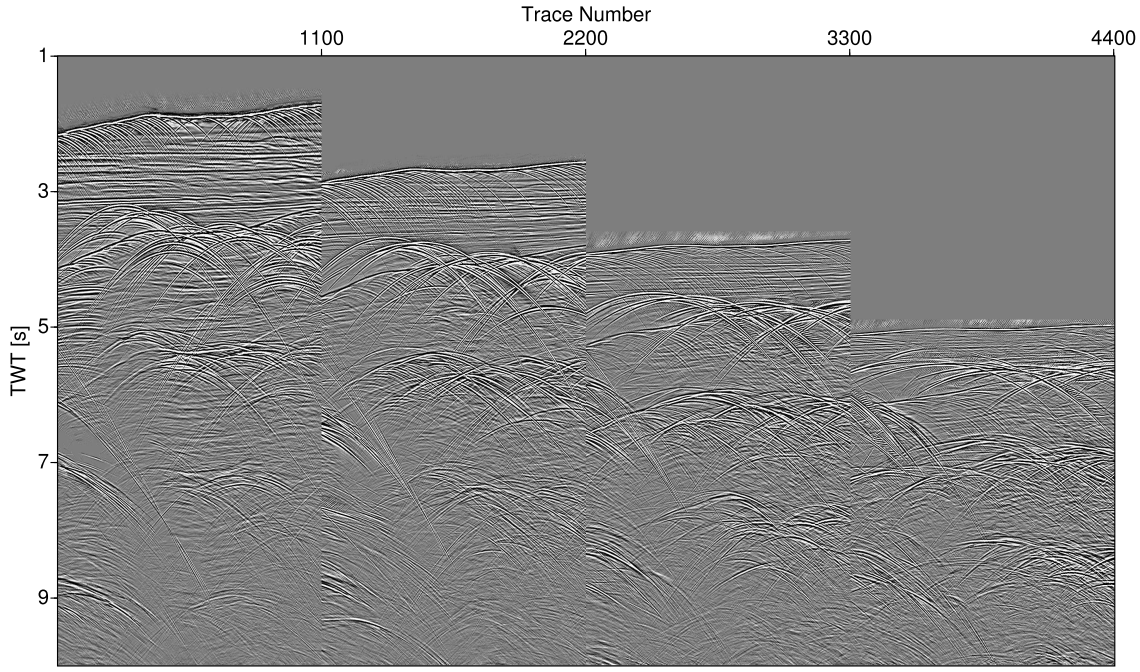

(a)

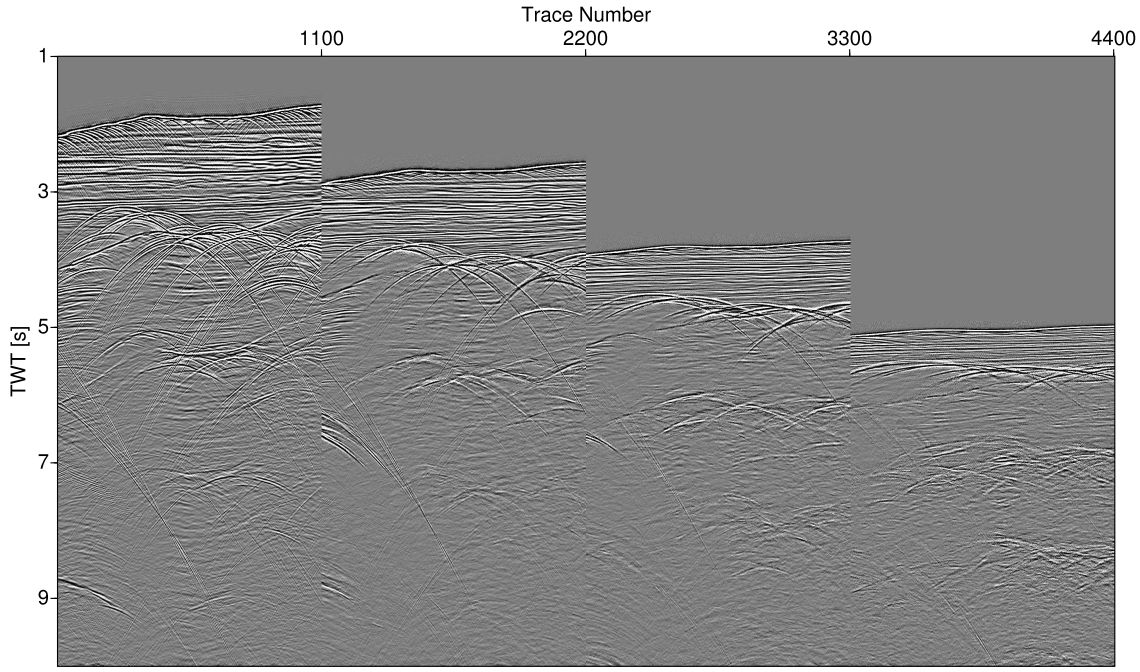

(b)

Figure 5: Excerpts of finite-offset stacked sections of the 2004 BP velocity benchmark data for four offsets from 1000 (left) to 7000 m (right) generated by application of the new diffraction traveltime decomposition approach (a) and the partial CRS method (b). The data was plotted with the same clip as the raw data displayed in Figure 4.

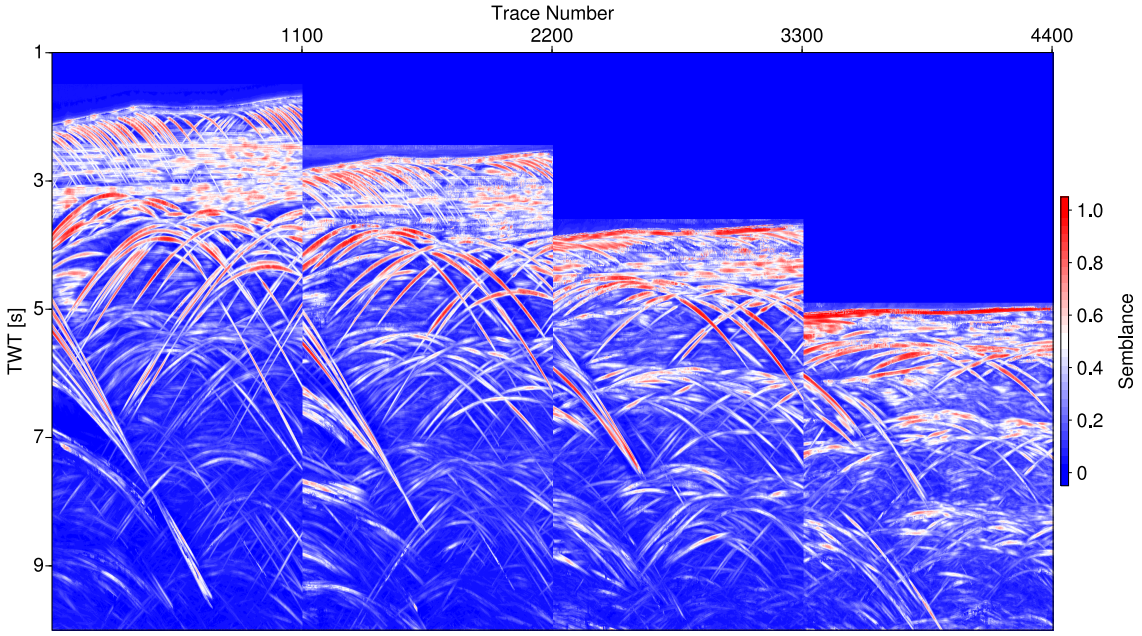

(a)

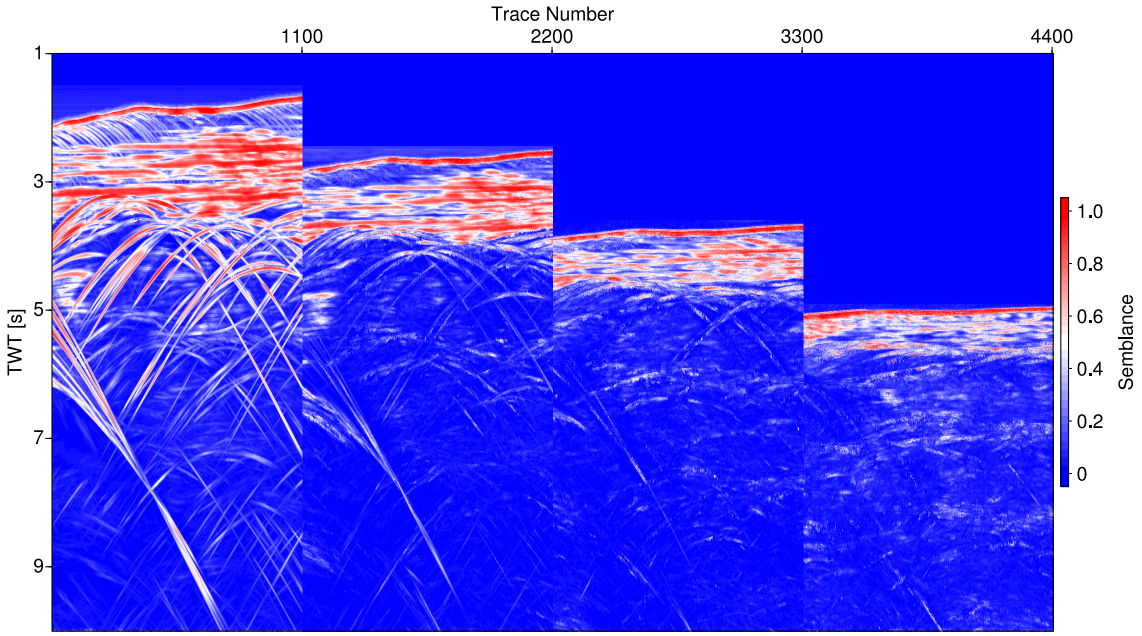

(b)

Figure 6: Excerpts of finite-offset semblance sections of the 2004 BP velocity benchmark data for four offsets from 1000 (left) to 7000 m (right) generated by application of the new diffraction traveltime decomposition approach (a) and the partial CRS method (b).

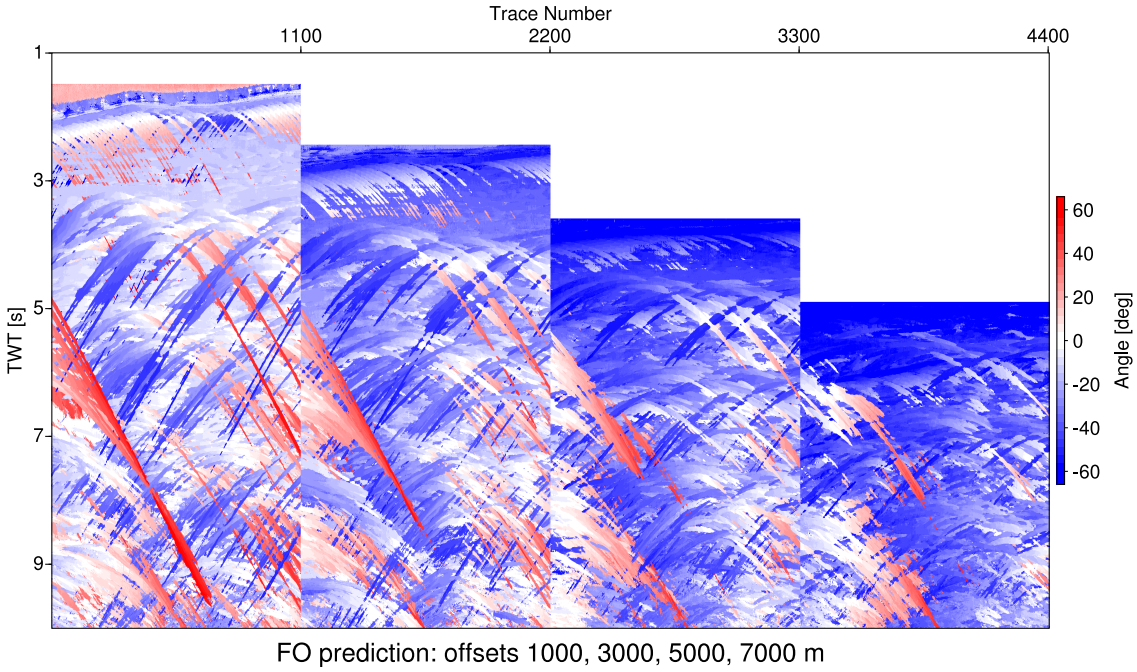

(a)

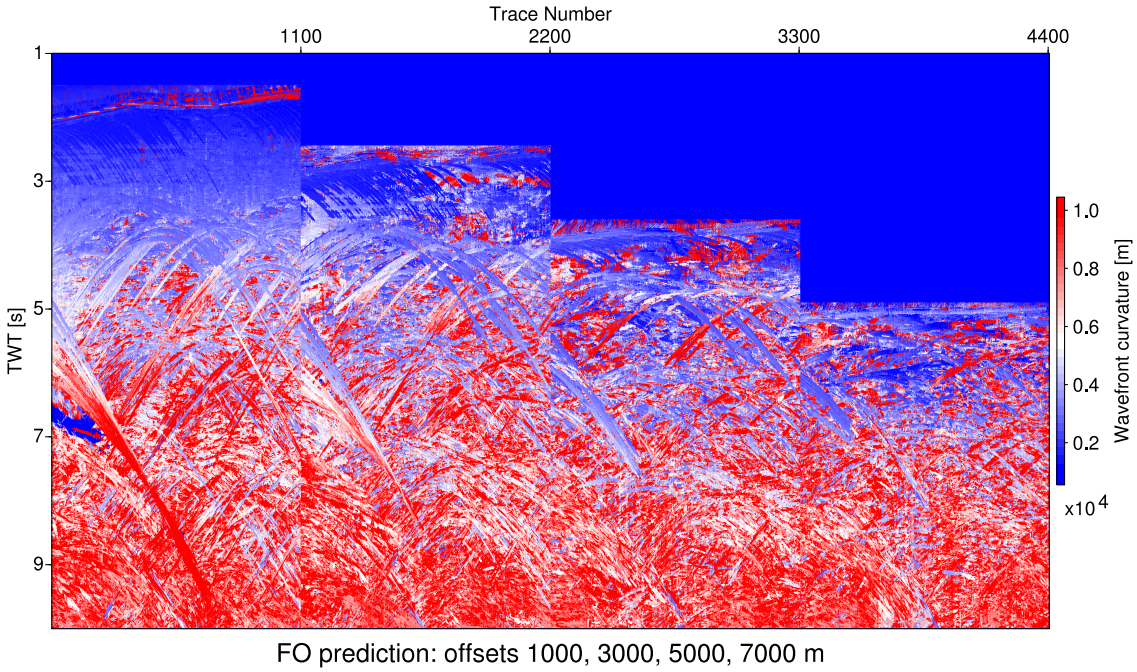

(b)

Figure 7: Excerpts of finite-offset source attribute sections α_s and R_s of the 2004 BP velocity benchmark data for four offsets from 1000 (left) to 7000 m (right) generated by application of the new diffraction traveltime decomposition approach.

of the stability of zero-offset processing, which is due to the smaller number of parameters compared to the more complex finite-offset setting.

CONCLUSIONS AND OUTLOOK

Based on our previous work (Bauer et al., 2014a,b, 2015), we have introduced a universal traveltime decomposition principle for diffractions, which is based on the decoupling of diffraction raypaths. This implies a kinematic symmetry, which makes zero-offset and finite-offset information redundant for diffractions. We found that every finite-offset diffraction operator can be decomposed into two independent zero-offset diffraction operators. In this fashion, we are able to image diffractions at arbitrary finite-offsets without loss of accuracy and solely based on zero-offset processing results.

In the context of the common-reflection-surface (CRS) stack (Jäger et al., 2001; Zhang et al., 2001), we enhanced our method by incorporating conflicting dips into the workflow. We used the traveltime decomposition principle to enhance prestack diffraction data and to obtain prestack diffraction wavefield attributes, which can be used for inversion. The results on simple waveform data showed the method's ability to fit diffractions at arbitrary offsets using only zero-offset attributes as input. Subsequent application to complex data confirmed the potential of the method for the enhancement of prestack diffraction data and attributes.

Since our method is entirely zero-offset based, it benefits from every improvement in the zero-offset processing. The use of zero-offset attributes obtained from a global optimization scheme with improved conflicting dip handling (Walda and Gajewski, 2015) has increased the quality of our results. Also, the application of non-hyperbolic operators such as i-CRS (Schwarz et al., 2014b) may lead to further improvement. Future work also includes the extension of the decomposition principle to 3D. For a point diffractor, this extension is straightforward. However, at structures such as edge or line diffractors, the decomposition principle is only applicable within that subset of directions, where the structure acts as a point diffractor. In addition, the unique properties of diffractions such as improved illumination and decoupling of raypaths are promising for the successful development of a diffraction-based tomographic scheme, which unites the efficiency of NIP-wave tomography (Duveneck, 2004) and the improved resolution of prestack stereotomography (Billette and Lambaré, 1998).

ACKNOWLEDGMENTS

This work was kindly supported by the sponsors of the *Wave Inversion Technology (WIT) Consortium*, Hamburg, Germany. We thank the applied seismics group at the University of Hamburg for continuous discussion. For the generation of the simple data example, the NORSAR-3D raytracing software was used. The BP 2004 velocity benchmark dataset was provided by Billette and Brandsberg-Dahl (2005).

REFERENCES

Bauer, A. (2014). From zero-offset to common-offset with diffractions. master's thesis, University of Hamburg.

Bauer, A., Schwarz, B., and Gajewski, D. (2014a). From ZO to CO with diffractions: Complex data examples. *18th Annual WIT report*.

Bauer, A., Schwarz, B., and Gajewski, D. (2014b). From ZO to CO with diffractions: Theory. *18th Annual WIT report*.

Bauer, A., Schwarz, B., and Gajewski, D. (2015). Prestack diffraction enhancement using a traveltime decomposition approach. *SEG Expanded Abstracts*, pages doi: 10.1190/segam2015–5847698.1.

Baykulov, M. and Gajewski, D. (2009). Prestack seismic data enhancement with partial common-reflection-surface (CRS) stack. *Geophysics*, 74(3):V49–V58.

Berkovitch, A., Belfer, I., Hassin, Y., and Landa, E. (2009). Diffraction imaging by multifocusing. *Geophysics*, 74(6):WCA75–WCA81.

Billette, F. and Brandsberg-Dahl, M. (2005). The BP 2004 velocity benchmark. In *67th EAGE Conference and Exhibition*.

Billette, F. and Lambaré, G. (1998). Velocity macro-model estimation from seismic reflection data by stereotomography. *Geophysical Journal International*, 135(2):671–690.

Dell, S. and Gajewski, D. (2011). Common-reflection-surface-based workflow for diffraction imaging. *Geophysics*, 76(5):S187–S195.

Duveneck, E. (2004). Velocity model estimation with data-derived wavefront attributes. *Geophysics*, 69(1):265–274.

Fomel, S., Landa, E., and Taner, M. T. (2007). Poststack velocity analysis by separation and imaging of seismic diffractions. *Geophysics*, 72(6):U89–U94.

Hubral, P. (1983). Computing true amplitude reflections in a laterally inhomogeneous earth. *Geophysics*, 48:1051–1062.

Jäger, R., Mann, J., Höcht, G., and Hubral, P. (2001). Common-reflection-surface stack: Image and attributes. *Geophysics*, 66:97–109.

Khaidukov, V., Landa, E., and Moser, T. J. (2004). Diffraction imaging by focusing-defocusing: An outlook on seismic superresolution. *Geophysics*, 69:1478–1490.

Mann, J. (2002). *Extensions and applications of the common-reflection-surface stack method*. PhD thesis, University of Karlsruhe.

Müller, T. (1999). *The common reflection surface stack method – seismic imaging without explicit knowledge of the velocity model*. PhD thesis, University of Karlsruhe.

Schwarz, B., Vanelle, C., and Gajewski, D. (2014a). From zero-offset to common-offset with diffractions. In *76th EAGE Conference and Exhibition - Workshops*.

Schwarz, B., Vanelle, C., Gajewski, D., and Kashtan, B. (2014b). Curvatures and inhomogeneities: an improved common-reflection-surface approach. *Geophysics*, 79(5):S231–S240.

Spinner, M., Tomas, C., Marchetti, P., Gallo, C., and Arfeen, S. (2012). Common-offset CRS for advanced imaging in complex geological settings. *SEG Expanded Abstracts*, pages doi: 10.1190/segam2012–1099.1.

Walda, J. and Gajewski, D. (2015). Common-reflection-surface stack improvement by differential evolution and conflicting dip processing. *SEG Expanded Abstracts*, pages doi: 10.1190/segam2015–5910957.1.

Yilmaz, O. (2001). *Seismic data analysis*. SEG, Tulsa.

Zhang, Y., Bergler, S., and Hubral, P. (2001). Common-reflection-surface (CRS) stack for common offset. *Geophysical Prospecting*, 49:709–718.